Supporting Information

Parikh et al. 10.1073/pnas.1204384109

SI Materials and Methods

Samples and Mutation Discovery. Human tumor samples with appropriate consent were obtained from commercial sources (Dataset S2). DNA from tumor (with >70% tumor content) and matched normal tissue was extracted using the Qiagen Tissue easy kit (Qiagen). All coding exons of AKT1, AKT2, and AKT3 were amplified and sequenced as described before (Dataset S6) (1). The somatic nature of the mutations was confirmed by DNA sequencingor MS analysis (Sequenom).

Molecular Modeling/Prediction. Potential sites for mutation were identified by inspection of the structure of full-length AKT1 (Protein Data Bank ID code 3O96) (2). A residue was deemed to be at the interface if atoms in a residue of one domain were within 5 Å of any atom in the other domain. Each interface position was considered for mutation if an amino acid change could perturb the pleckstrin homology (PH) –kinase domain (KD) interaction by either introduction of an unfavorable contact (steric or polar) or removal of some favorable interaction (hydrophobic or polar). Several other sites were also included in the mutagenesis library if side chains were close to the interdomain interface, KD residues that were part of missing loops in the KD proximal to the PH domain, or PH domain residues potentially close to these missing KD loops. For example, electron density is not observed for the 189–199 loop in the full-length AKT1 structure, and the location of its termini suggests that the loop is likely in proximity to the PH domain. Because there is a large conformational change between the inactive and active KD of AKT1 (2), interface residues were not considered for mutation if the corresponding change might compromise the activity of the active KD. The structure of the activated KD of AKT1 was used for this purpose (Protein Data Bank ID code 3OW4).

Homology models of full-length AKT2 and AKT3 were constructed using the AKT1 structure as a template. The models were constructed using the modeling package MOE (version 2011.11) using the default settings in the Homology Model tool. The resulting models were minimized using the AMBER99 force field in the presence of the allosteric inhibitor. The same process was used to model loops for AKT1 not present in the deposited structure (Fig. 2*B*). Protein alignments, visual inspections of the models, and generation of structure figures were performed using PyMOL (PyMOL Molecular Graphics System, version 1.5.0.1; Schrödinger, LLC).

Activating *AKT* Mutation Screen. Sequencing libraries were created from PCR-amplified AKT coding sequence with TruSeq DNA Sample Prep Kit v2 (Illumina). Gel-purified PCR products (1 μg in 50 μL 10 mM Tris·Cl, pH 8.5) were sheared to an average size of 225 bp using a Covaris E210 (Covaris) with the following settings: duty cycle 10%, intensity 5, and cycles/burst 200. The TruSeq DNA Sample Prep Kit gel-free protocol was used for end repair, polyadenylation, adapter ligation, and PCR amplification. Libraries were quantified using the Kapa Library Quant Kit (Kapa Biosystems) on a Viia7 Real-Time PCR System (Life Technologies). Libraries were pooled and sequenced in a single lane of a flow cell on the Illumina HiSeq2000 using v3 chemistry, yielding a total of 167 million reads. Single-end 75-bp reads were aligned to the AKT sequence using bwa with default settings (3). For each position along the AKT sequence, the nucleotides observed were counted using only high-quality bases (Q score > 30). The frequency of each mutation was calculated as the number of observed mutants divided by the total number of observations at that position. For each time point, a frequency ratio was calculated by dividing the frequency of each mutation by that mutation's frequency in the input. These ratios were normalized to the ratio of the WT control.

Cell Lines. NIH 3T3 fibroblasts were maintained in DMEM supplemented with 10% (vol/vol) FBS (Thermo Fisher), 2 mM L-glutamine, 100 U/mL penicillin, and 100 mg/mL streptomycin. MCF10A mammary epithelial cells were cultured in DMEM/F12 supplemented with 5% (vol/vol) donor horse serum, 20 ng/mL EGF, 10 μg/mL insulin, 100 μg/mL hydrocortisone, 1 ng/mL cholera toxin, 50 U/mL penicillin, and 50 mg/mL streptomycin. BaF3 cells were cultured in RPMI 1640 supplemented with 10% (vol/vol) FBS, 2 mM L-glutamine, 100 U/mL penicillin, 100 mg/mL streptomycin, and 2 ng/mL recombinant murine IL-3 (R&D Systems).

Plasmids. N-terminally FLAG-tagged *AKT1*, *AKT2*, and *AKT3* (WT) were constructed using standard PCR techniques and cloned into pRetro-internal ribosome entry site (IRES)-GFP vector (Clontech). Myristoylated (Myr) -*AKT1*, *AKT2*, and *AKT3* were constructed by fusing an N-terminal myristoyl sequence and a C-terminal FLAG-tag. *AKT1*, *AKT2*, and *AKT3* mutants were generated by using the QuikChange Site-Directed Mutagenesis Kit (Stratagene) and cloned into the pRetro-IRES-GFP vector. Activated MEK1 (Mek1 ΔN3, S218E, S222D) was constructed as previously described (4) and cloned into the pMXs-puro retroviral vector (Cell Biolabs).

Generation of Stable Cell Lines. Retroviral constructs expressing WT or mutant AKT1, AKT2, and AKT3 were transfected into the Phoenix amphoteric packaging cell line using Fugene6 (Roche). The viral supernatant was harvested 48 h after transfection and filtered using a 0.45-μM syringe filter. The virus was used to infect NIH323, MCF10A, and BaF3 cells by spinoculation (1,800 rpm for 45 min), and the infected cells were sorted by flow cytometry based on GFP fluorescence. To generate stable cell lines expressing active MEK1 alone or combined with AKT1, AKT2, or AKT3, FACS-sorted AKT expressing cells or parental BaF3 cells were infected with MEK1 N3 virus, and infected cells were selected with puromycin (2 μg/mL) for 7 d. Pools of these cells were used for additional studies.

Live-Cell Imaging. NIH 3T3 cells stably expressing GFP-AKT1 pleckstrin homology domain (PHD) (WT, E17K, or L52R) fusions were plated on cover glass and serum-starved for 18 h. Cells were stimulated with 30 ng/mL PDGF (R&D Systems) for 10 min and imaged using an Olympus DSU Time Lapse microscope at 30-s intervals for a total of 15 min.

Recombinant Proteins. We used *Escherichia coli* to generate recombinant AKT1 PH domain and baculovirus to generate AKT1 KD.
Expression. BL-21 *E. coli* cells were transformed with pET32A-AKT1 PHD (residues 1–123) expression constructs and induced with 0.5 mM IPTG [Isopropyl β-D-1-thiogalactopyranoside TCEP-Tris(2-carboxyethyl)phosphine] overnight at 16 °C to express 6× HIS-tagged proteins. Postinduction, cells were centrifuged at 4,648 × *g* for 10 min at 4 °C and pelleted. Recombinant baculoviruses that expressed AKT1 KD (WT or D323H) were made using the baculovirus expression system (Orbigen); 1 L Sf9 insect cells, at a density of 2×10^6 cells/mL, was infected with WT or D323H AKT1 KD (118–480) virus at a multiplicity of infection of 0.5. The cells were cultured at 27 °C for 72 h and harvested by centrifugation.

Purification. Cells were lysed using a lysis buffer (50 mM Tris, pH 8, 150 mM NaCl, 1 mM TCEP, 20 mM Imidazole, and EDTA free Complete protease inhibitor mixture tablets; Roche). The cell lysate was centrifuged at 40,000 rpm for 1 h at 4 °C to separate the soluble and insoluble fractions. The supernatant containing the soluble fraction was loaded over an Ni-NTA column preequilibrated with 20 mM Tris, pH 8, 20 mM Imidazole, 300 mM NaCl, and 0.5 mM TCEP. The HIS-tagged protein was then eluted with 1 column volume 20 mM Tris, pH 8.0, 250 mM Imidazole, 300 mM NaCl, and 0.5 mM TCEP. A Superdex 200 16/60 column (GE Healthcare) was used to further purify AKT. The buffer used for the size exclusion column was 25 mM Hepes, pH 7, 100 mM NaCl, 10% (vol/vol) Glycerol, and 0.25 mM TCEP.

Western Blot. NIH 3T3, BaF3, or MCF10A cells stably expressing the appropriate mutants were lysed in radio immuno precipitation assay (RIPA) buffer (50 mM Tris·HCl, 150 mM NaCl, 1 mM EDTA, and 1% Triton X-100) and boiled at 100 °C for 5 min. Lysates from 3D cultures were prepared as described previously (5). The lysates were clarified by centrifugation, resolved on 4–20% polyacrylamide gels (Invitrogen), and transferred to nitrocellulose membranes. The membranes were probed with the primary antibodies indicated followed by appropriate HRP-conjugated secondary antibodies.

Antibodies against phosphorylated AKT (pAKT; T308), pAKT (S473), AKT, pS6RP, S6RP, pPRAS40, PRAS40, pFOXO, and FOXO were purchased from Cell Signaling Technologies. Anti-FLAG antibody (M2) and β-ACTIN were purchased from Sigma-Aldrich.

Western blot bands were quantified using the densitometry software ImageJ (6). For each mutant, pAKT level was computed as the ratio of pAKT over total AKT (FLAG), and this level was normalized to the levels of ACTIN. We tested the correlation between the pAKT levels and a $\log_{10}$-normalized ratio of IL-3–independent survival activity of the mutants using the lm function in R version 2.11.1.

3D Morphogenesis Assay. MCF10A cells stably expressing WT, Myr, or mutant AKT1 were seeded on growth factor-reduced Matrigel (BD Biosciences) in eight-well chamber slides (BD Falcon) as described previously (5). Assay medium [F12/DMEM supplemented with 2% (vol/vol) horse serum, 0.5 μg/mL hydrocortisone, 0.1 μg/mL cholera toxin, 5 ng/mL EGF, and 10 μg/mL insulin] was replaced every 3–4 d. Acini were visualized and imaged on an Olympus IX81 inverted microscope.

Soft Agar Colony Formation Assay. NIH 3T3 cells stably expressing WT, Myr, or mutant AKT1 were suspended in 2× DMEM supplemented with 20% (vol/vol) FBS and mixed 1:1 with 0.7% agarose (final concentration = 0.35%), which was overlaid on 0.5% base agar in six-well plates and incubated at 37 °C for 3–4 wk. Cultures were supplemented with fresh media every 2–3 d. ImageXpress software (Molecular Devices) was used to compute the colony count. Soft agar assays were done in triplicate and repeated at least two times.

Mammalian Two-Hybrid Assay. Mammalian two-hybrid interaction assays were performed using the Matchmaker Mammalian Assay kit (Clontech) as per manufacturer instructions. Briefly, HeLa cells were cotransfected with combinations of Gal4BD-AKT1 KD (WT or mutant) as bait, VP16AD-AKT1 PH domain (WT or mutant) as prey, and the reporter vector, pG5SEAP. SEAP protein was measured using the Great EscAPe SEAP Chemiluminescence Detection Kit (Clontech).

NIH 3T3 Proliferation Assay. NIH 3T3 cells stably expressing WT or mutant AKT1 were seeded in a 384-well plate at 1,000 cells/well and incubated overnight at 37 °C under 5% CO_2. AKT inhibitors were added to the cells at a concentration of 2 μM, and cell viability was measured using the CellTiter-Glo luminescence cell viability kit (Promega), 4 d after addition of the inhibitors.

IL-3–Independent Survival Assay. BaF3 cells stably coexpressing MEK1 N3 (ΔN3, S218E, S222D) and WT or mutant AKT1 were washed three times with 1× PBS and plated in 96-well plates (5,000 cells/well) in replicates of 8–12 in complete RPMI medium without IL-3. Cell viability was measured using the Cell Titer Glo Luminescence Cell Viability Kit (Promega), and plates were read on a Synergy 2 (Biotek Instruments) luminescence plate reader. For each time point, the viable cell number value was normalized against the corresponding 0-h value.

Animal Studies. BaF3 cells (1×10^6) expressing empty vector, WT, or mutant AKT1 together with activated MEK1 were injected into tail veins of 8- to 12-wk-old Balb/C nude mice. Each treatment arm had a total of 13 animals, of which 3 animals were subjected to timed necropsies (at day 19) to assess disease progression, whereas the remaining 10 animals were followed for survival. Flow cytometry analysis was performed on cells from the bone marrow and spleen to detect the presence of GFP fluorescence. For histological analyses, 4-μM-thick sections were sliced from formalin-fixed, paraffin-embedded tissues and stained with H&E (Sigma). Histology slides were observed under a Nikon 80i compound microscope and images captured with a Nikon DS-R camera. All animal studies were performed under Genentech's Institutional Animal Care and Use Committee approved protocols.

AKT1 Activity Assay. AKT1 kinase activity was determined in an assay buffer consisting of 10 mM Tris·Cl, pH 7.5, 1 mg/mL bovine γ-globulins, and 1 mM DTT. In experiments including AKT inhibitors, AKT1 protein was preincubated with inhibitors at room temperature for 10 min in assay buffer. The kinase catalytic activity was then determined with 20 nM AKT1 enzyme in 50 μL final volume of assay buffer containing 50 μM Crosstide (Millipore), 50 μM [33P] ATP (1 μCi per assay; PerkinElmer), and 5 mM $MgCl_2$. On the addition of both substrates, the reaction was incubated at room temperature for 30 min. AKT1 kinase activity was terminated with 200 mM phosphoric acid at the end of incubation. Phosphoric acid-treated P81 filter paper was used to capture [33P]-labeled Crosstide. Filter papers were washed with 5% (vol/vol) phosphoric acid three times after trapping the radioactive product. The radioactivity embedded in the filter papers was quantified with a scintillation counter and used for calculating AKT enzyme activity. For experiments using reconstituted AKT-PH and KDs, the PH domain and the KD were reconstituted by combining the domains in a molar ratio of 10:1 at room temperature for 5 min in assay buffer before the assay.

1. Jaiswal BS, et al. (2009) Somatic mutations in p85alpha promote tumorigenesis through class IA PI3K activation. *Cancer Cell* 16(6):463–474
2. Wu WI, et al. (2010) Crystal structure of human AKT1 with an allosteric inhibitor reveals a new mode of kinase inhibition. *PLoS One* 5(9):e12913.
3. Li H, Durbin R (2009) Fast and accurate short read alignment with Burrows-Wheeler transform. *Bioinformatics* 25(14):1754–1760.
4. Mansour SJ, et al. (1994) Transformation of mammalian cells by constitutively active MAP kinase kinase. *Science* 265(5174):966–970.
5. Lee GY, Kenny PA, Lee EH, Bissell MJ (2007) Three-dimensional culture models of normal and malignant breast epithelial cells. *Nat Methods* 4(4):359–365.
6. Schneider CA, Rasband WS, Eliceiri KW (2012) NIH Image to ImageJ: 25 years of image analysis. *Nat Methods* 9(7):671–675.

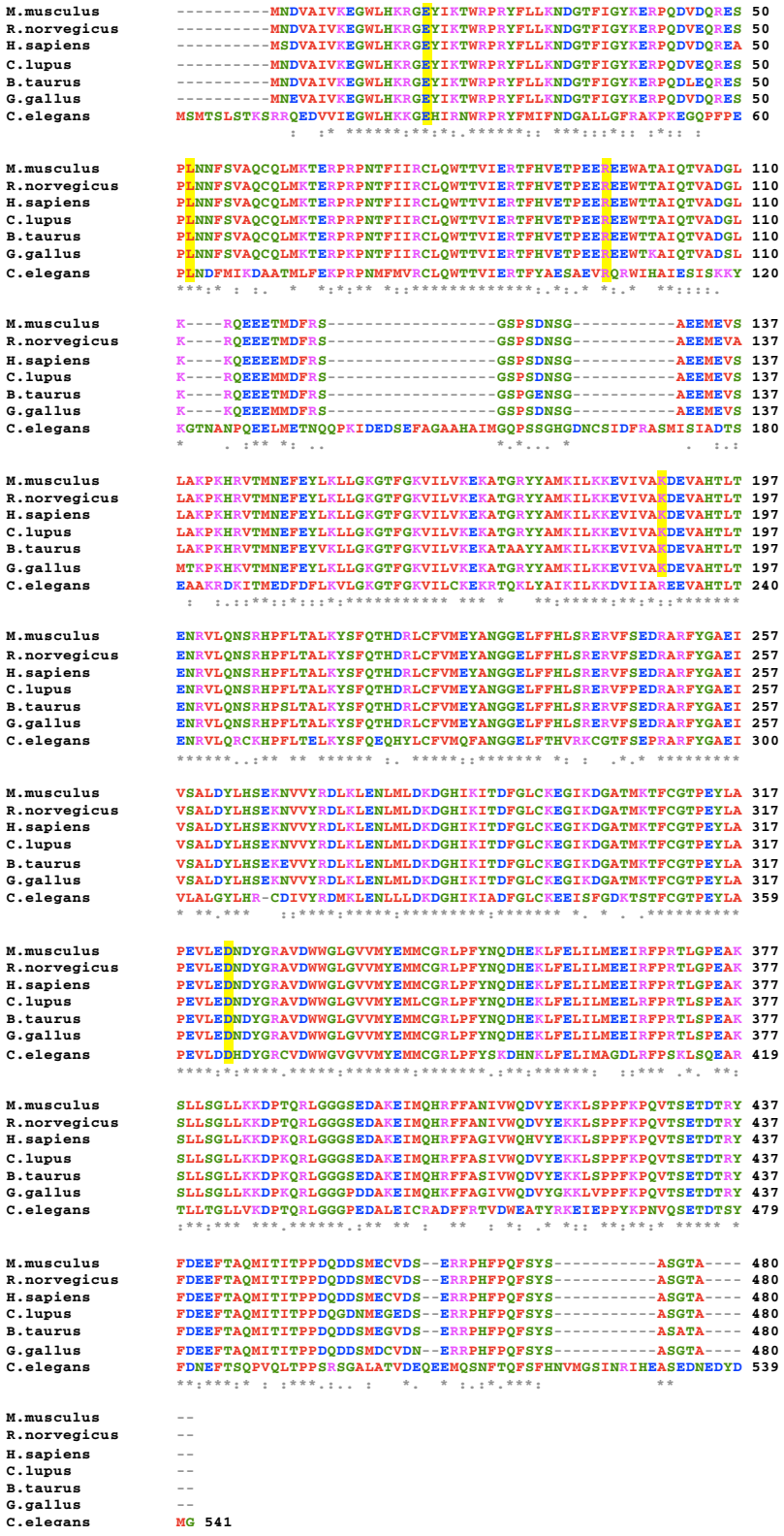

Fig. S1. Multiple sequence alignment of AKT1 orthologs. *Homo sapiens* (NP_001014431.1), *Canis lupus* (XP_548000.2), *Bos taurus* (NP_776411.1), *Mus musculus* (NP_033782.1), *Gallus gallus* (NP_990386.1), *Rattus norvegicus* (NP_150233.1), and *Caenorhabditis elegans* (NP_001023645.1) AKT1 sequences aligned using ClustalW (1). Somatic mutations are highlighted in yellow.

1. Larkin MA, et al. (2007) Clustal W and Clustal X version 2.0. *Bioinformatics* 23(21):2947–2948.

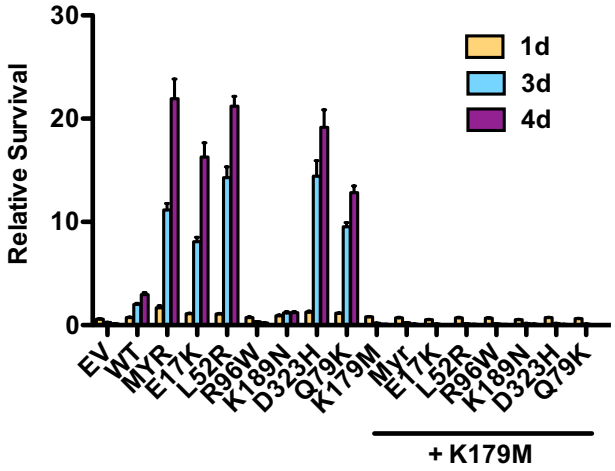

Fig. S2. IL-3–independent survival of BaF3 cells expressing the indicated *AKT1* mutants and their kinase dead (K179M) versions.

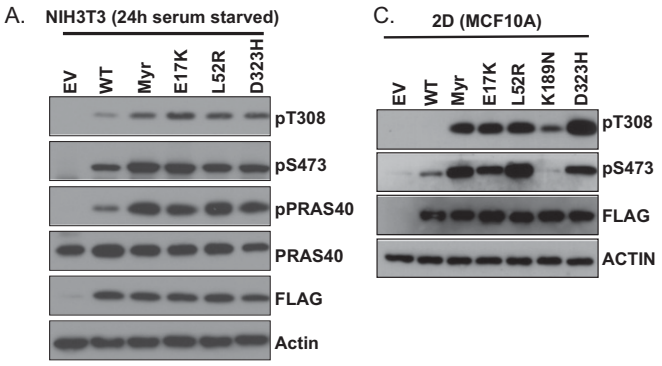

B.

AKT	Fold pPRAS40 levels/WT*
WT	1.0
MYR	3.73
E17K	3.12
L52R	3.69
D323H	4.76

* Normalized to total PRAS40 and Actin

Fig. S3. (*A*) Immunoblot analysis of NIH 3T3 cells expressing *AKT1* mutants. (*B*) Quantification of levels of pPRAS40 shown in *A*. (*C*) Immunoblot analysis of MCF10A cells expressing indicated *AKT1* mutants cultured in monolayer (2D).

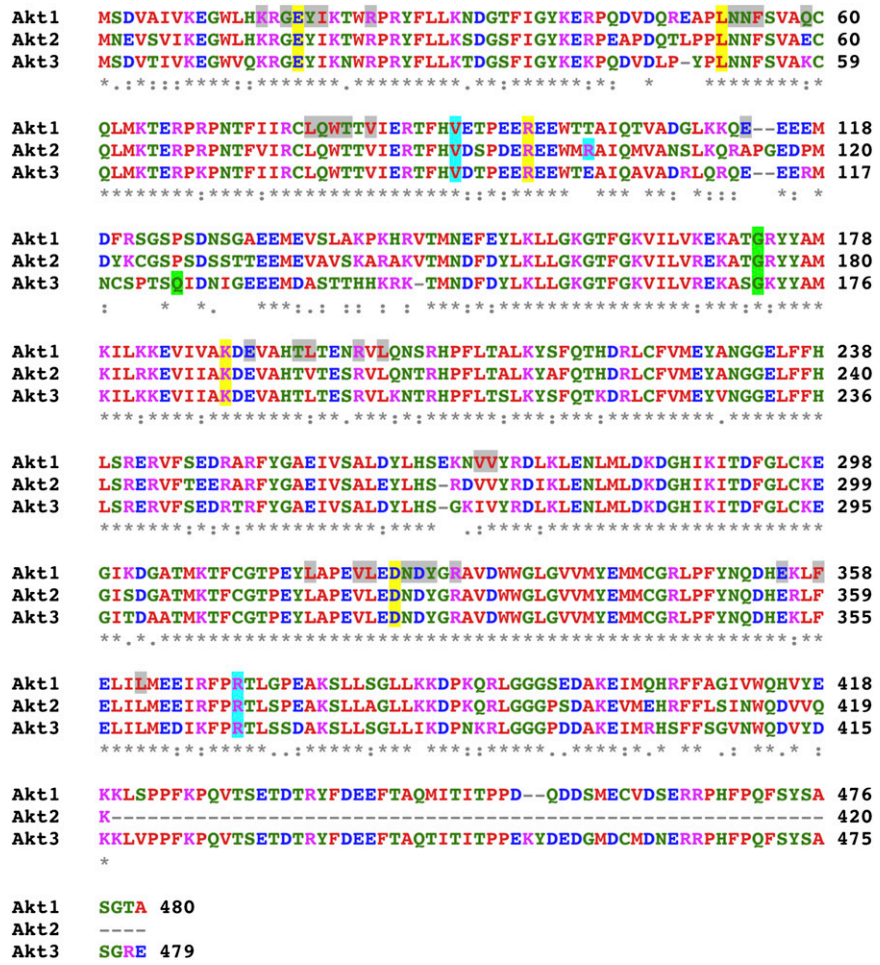

Fig. S4. Multiple sequence alignment of human AKT1 (NP_001014431.1), AKT2 (NP_001617.1), and AKT3 (NP_005456.1). Somatic mutations identified in AKT1 (yellow), AKT2 (blue), and AKT3 (green) are shown. AKT1 residues shaded in gray represent synthetic mutants used in the screen depicted in Fig. 1.

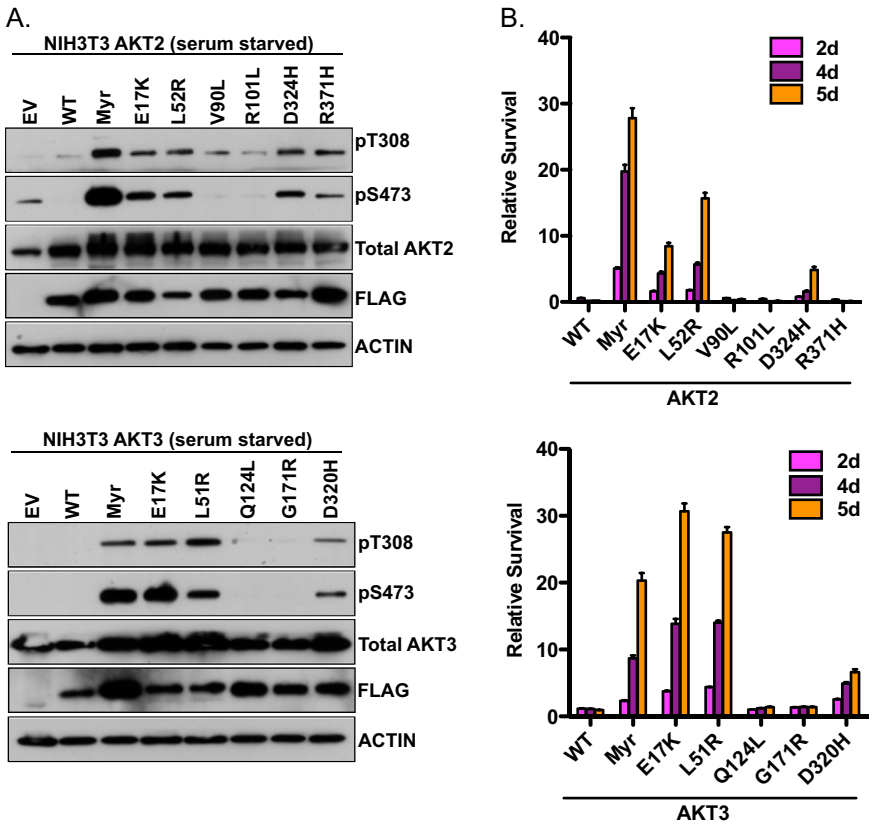

Fig. S5. Disruption of AKT2 and AKT3 PH–KD interactions leads to activation. (*A*) Immunoblot analysis of the activation status of *AKT2* or *AKT3* mutants in NIH 3T3 cells. (*B*) IL-3–independent survival of BaF3 cells expressing *AKT2* or *AKT3* mutants.

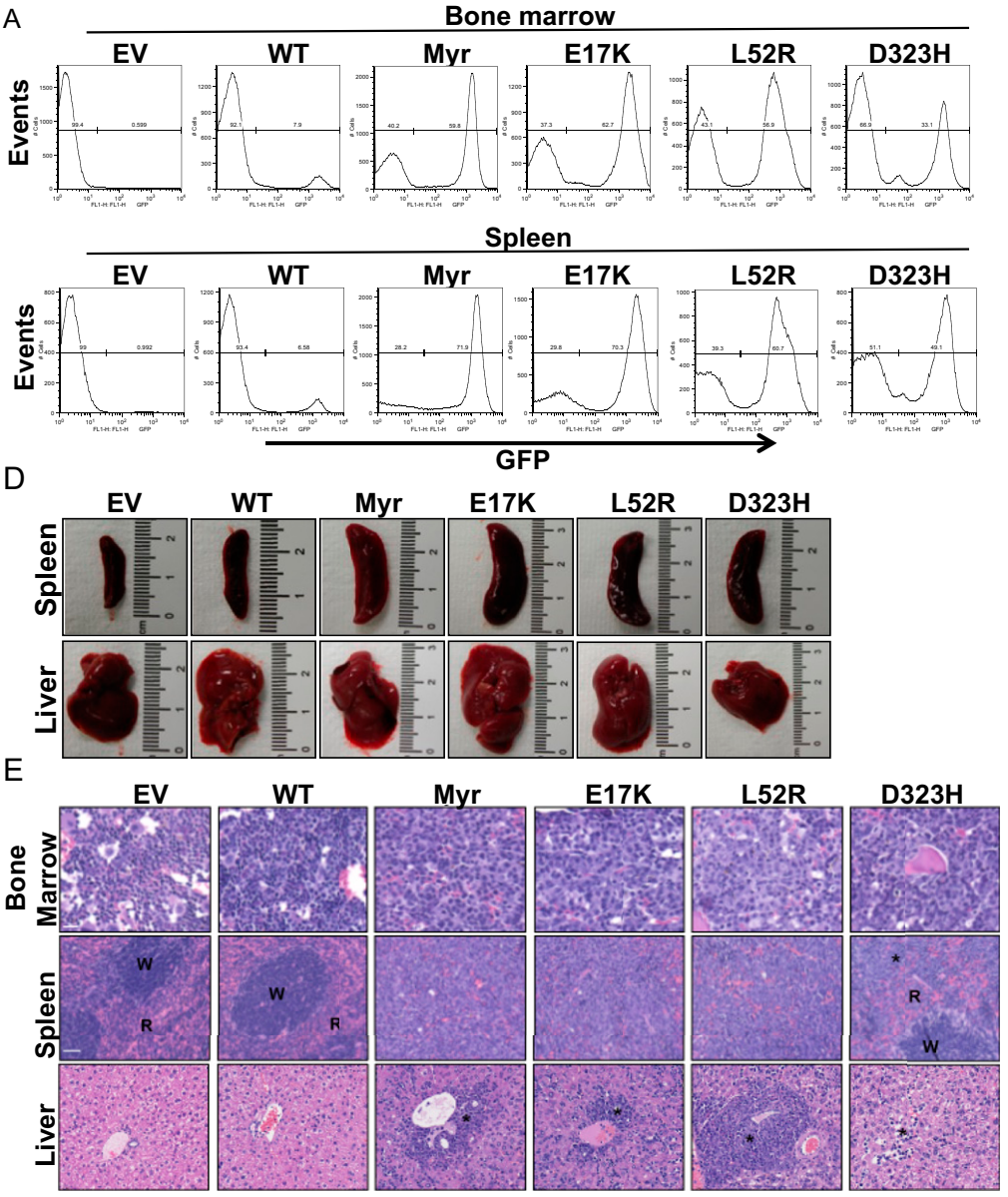

Fig. S6. (*A*) Representative flow cytometric plots of bone marrow and spleen from mice receiving GFP-tagged BaF3 cells expressing *AKT1* mutants. (*B*, *C*) Mean spleen and liver weight on day 19 from mice implanted with *AKT1* mutants. (*D*) Representative images of spleen and liver from mice transplanted with BaF3 cells expressing *AKT1* mutants. (*E*) Representative H&E-stained bone marrow, spleen, and liver sections from mice analyzed in *A*. *Tumor cell infiltration in the liver. R, red pulp; W, white pulp. (Scale bar: bone marrow, 20 μm; spleen and liver, 40 μm.)

Structure of GNE-929

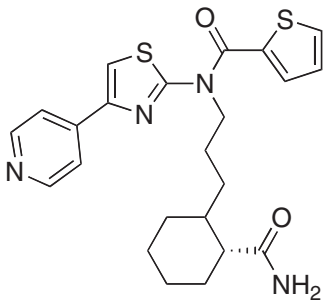

Fig. S7. Structure of GNE-929.

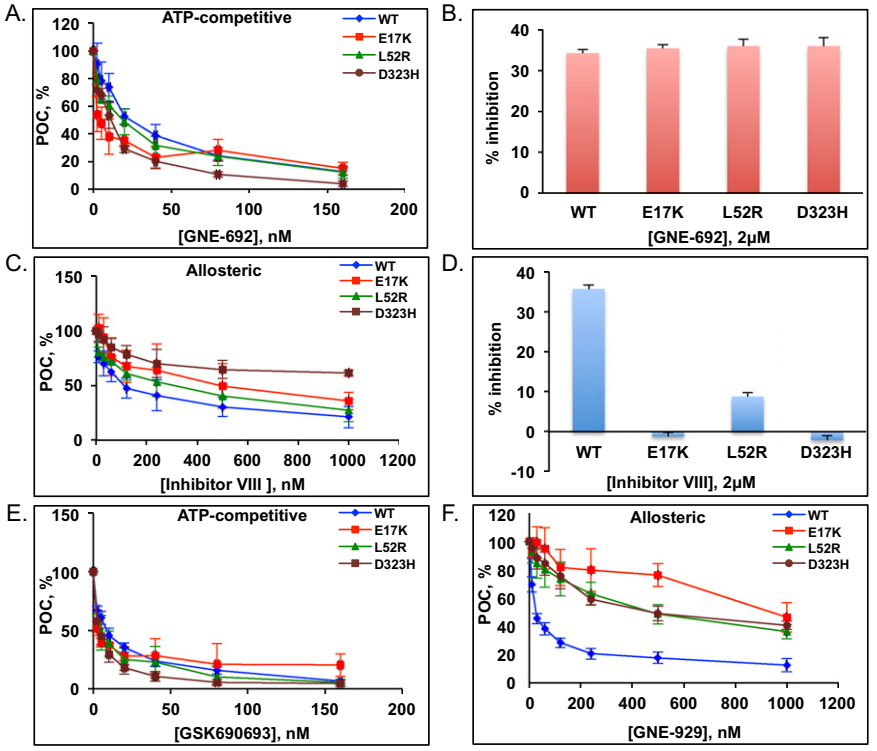

Fig. S8. (*A*–*D*) Effect of ATP-competitive inhibitor GNE-692 (*A* and *B*) or allosteric AKT inhibitor Inhibitor VIII (*C* and *D*) on activity of recombinant full-length AKT1 (*A* and *C*) or proliferation of NIH 3T3 cells expressing AKT1 (*B* and *D*). Error bars represent SE of quadruplets. Representative data from at least three experiments are shown. (*E*) Effect of ATP-competitive inhibitor GSK690693 and (*F*) allosteric AKT inhibitor GNE-929 on recombinant full-length WT or mutant AKT1.

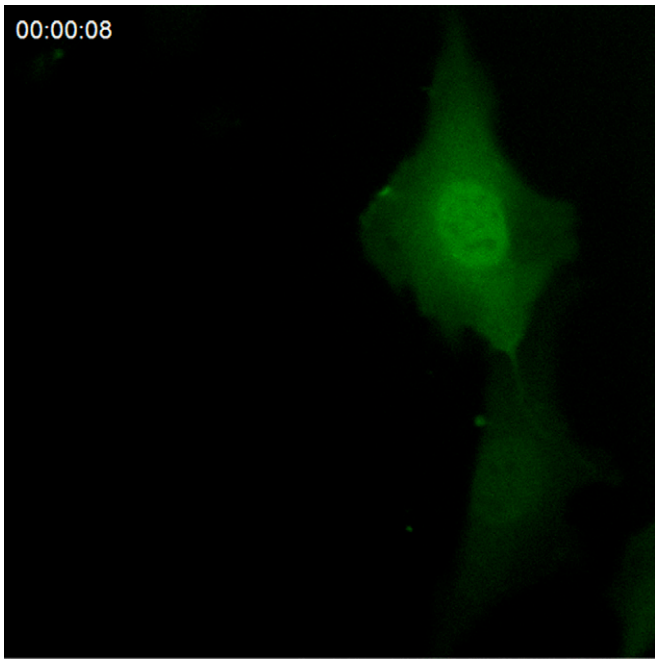

Movie S1. Live-cell imaging of GFP-AKT1 WT PH domain in NIH 3T3 cells after stimulation with PDGF.

Movie S1

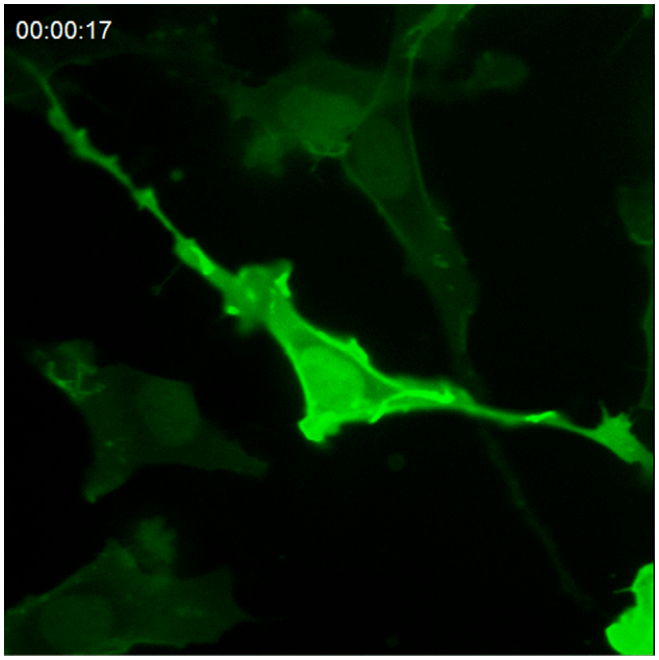

Movie S2. Live-cell imaging of GFP-AKT1 E17K PH domain in NIH 3T3 cells after stimulation with PDGF.

Movie S2

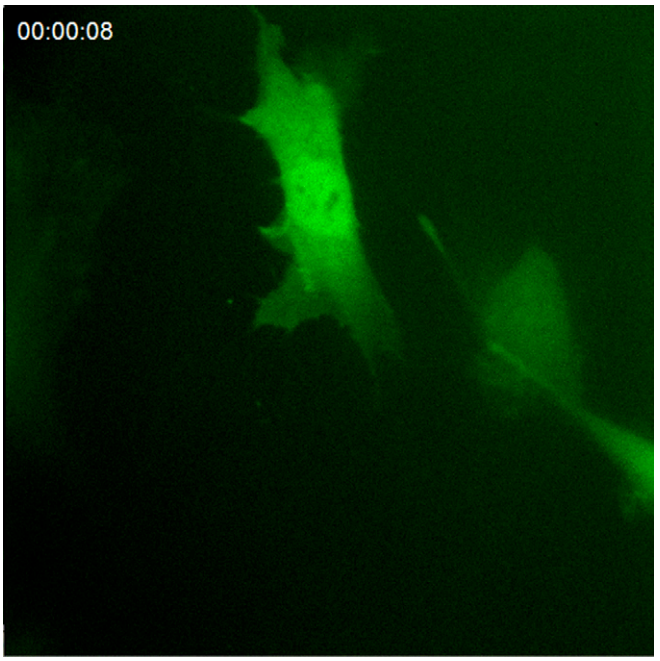

Movie S3. Live-cell imaging of GFP-AKT1 L52R PH domain in NIH 3T3 cells after stimulation with PDGF.

Movie S3

Other Supporting Information Files

Dataset S1 (XLS)
Dataset S2 (XLS)
Dataset S3 (XLS)
Dataset S4 (XLS)
Dataset S5 (XLS)
Dataset S6 (XLS)